Chinese Physics Letters **40**, 060301 (2023) **Express Letter**

Digital Simulation of Projective Non-Abelian Anyons with 68 Superconducting Qubits

Shibo Xu[1†], Zheng-Zhi Sun[2†], Ke Wang[1†], Liang Xiang[1], Zehang Bao[1], Zitian Zhu[1], Fanhao Shen[1], Zixuan Song[1], Pengfei Zhang[1], Wenhui Ren[1], Xu Zhang[1], Hang Dong[1], Jinfeng Deng[1], Jiachen Chen[1], Yaozu Wu[1], Ziqi Tan[1], Yu Gao[1], Feitong Jin[1], Xuhao Zhu[1], Chuanyu Zhang[1], Ning Wang[1], Yiren Zou[1], Jiarun Zhong[1], Aosai Zhang[1], Weikang Li[2], Wenjie Jiang[2], Li-Wei Yu[3], Yunyan Yao[1], Zhen Wang[1,4], Hekang Li[1], Qiujiang Guo[1,4], Chao Song[1,4*], H. Wang[1,4*], and Dong-Ling Deng[2,4,5*]

[1]*School of Physics, ZJU-Hangzhou Global Scientific and Technological Innovation Center, Interdisciplinary Center for Quantum Information, and Zhejiang Province Key Laboratory of Quantum Technology and Device, Zhejiang University, Hangzhou 310027, China*
[2]*Center for Quantum Information, IIIS, Tsinghua University, Beijing 100084, China*
[3]*Theoretical Physics Division, Chern Institute of Mathematics and LPMC, Nankai University, Tianjin 300071, China*
[4]*Hefei National Laboratory, Hefei 230088, China*
[5]*Shanghai Qi Zhi Institute, Shanghai 200232, China*

(Received 6 May 2023; accepted manuscript online 8 May 2023)

Non-Abelian anyons are exotic quasiparticle excitations hosted by certain topological phases of matter. They break the fermion-boson dichotomy and obey non-Abelian braiding statistics: their interchanges yield unitary operations, rather than merely a phase factor, in a space spanned by topologically degenerate wavefunctions. They are the building blocks of topological quantum computing. However, experimental observation of non-Abelian anyons and their characterizing braiding statistics is notoriously challenging and has remained elusive hitherto, in spite of various theoretical proposals. Here, we report an experimental quantum digital simulation of projective non-Abelian anyons and their braiding statistics with up to 68 programmable superconducting qubits arranged on a two-dimensional lattice. By implementing the ground states of the toric-code model with twists through quantum circuits, we demonstrate that twists exchange electric and magnetic charges and behave as a particular type of non-Abelian anyons, i.e., the Ising anyons. In particular, we show experimentally that these twists follow the fusion rules and non-Abelian braiding statistics of the Ising type, and can be explored to encode topological logical qubits. Furthermore, we demonstrate how to implement both single- and two-qubit logic gates through applying a sequence of elementary Pauli gates on the underlying physical qubits. Our results demonstrate a versatile quantum digital approach for simulating non-Abelian anyons, offering a new lens into the study of such peculiar quasiparticles.

DOI: 10.1088/0256-307X/40/6/060301

Quantum theory classifies all fundamental particles in nature as either bosons or fermions.[1] For instance, photons are bosons and electrons are fermions. This dichotomy classification has profound implications and plays a crucial role in understanding a variety of physical phenomena, ranging from metal-insulator transitions[2] to superconductivity[3] and Bose–Einstein condensation.[4] However, in two dimensions it is possible that emergent particles (quasiparticles) would circumvent this dichotomy principle and obey anyonic statistics,[5] where their exchange of positions would result in a generic phase factor that is neither 0 nor π (as for bosons or fermions), or even a unitary operation that shifts the system between different topologically degenerate states.[6] These quasiparticles are dubbed anyons.[7]

While braiding Abelian anyons only leads to a phase factor, braiding non-Abelian anyons would lead to a unitary transformation.[6–10] This prominent property gives rise to the notion of topological quantum computation,[6,11–14] where quantum information is encoded nonlocally and quantum computations are implemented by braiding and fusing non-Abelian anyons. The nonlocal encoding and the topological nature of braiding make topological quantum computation naturally immune to local errors, thus providing intrinsic fault tolerance at the level of hardware. However, despite numerous theoretical proposals for realizing non-Abelian anyons with a wide range of systems,[15–27] including fractional quantum Hall states,[9,23] cold atoms,[28] topological superconductors,[22] and Majorana zero modes,[21] the direct experimental observation of non-Abelian anyons and their braiding statistics still remains elusive so far.[29–32] Meanwhile, recent developments with quantum processors have demonstrated vast potential in simulating exotic

†These authors contributed equally to this work.
*Corresponding authors. Email: chaosong@zju.edu.cn; hhwang@zju.edu.cn; dldeng@tsinghua.edu.cn
© 2023 Chinese Physical Society and IOP Publishing Ltd

phases of matter [33–37] and demonstrating quantum error-correcting codes, [38–41] giving rise to intriguing opportunities for simulating and exploring non-Abelian anyons with these highly controllable systems. [42]

In this Letter, we report an experimental quantum digital simulation of projective non-Abelian anyons and their nontrivial braiding statistics with two superconducting processors (labeled as Ⅰ and Ⅱ), which are designed to carry arrays of 11×11 and 6×6 frequency-tunable transmon qubits, respectively. We select 68 (30) qubits on processor Ⅰ (Ⅱ) featuring a median lifetime of 109.8 μs (139.8 μs), and median fidelities of simultaneous single- and two-qubit gates above 99.91% and 99.4% (99.95% and 99.5%), respectively, for carrying out our experiments. We prepare the twisted toric-code ground states through efficient quantum circuits with a depth up to 43. We demonstrate that the twists exchange electric and magnetic charges when an odd number of them are winded around, and their braiding and fusion rules resemble that of Ising-type anyons. In addition, we show that these twists can be explored to encode topological logical qubits, and both single- and two-qubit logic gates can be implemented by applying a sequence of elementary Pauli gates on the physical superconducting qubits. Based on this, we are able to prepare a logical two-qubit Bell state on processor Ⅰ and a logical three-qubit Greenberger–Horne–Zeilinger (GHZ) state on processor Ⅱ, showing the existence of multipartite entanglement among the logical qubits.

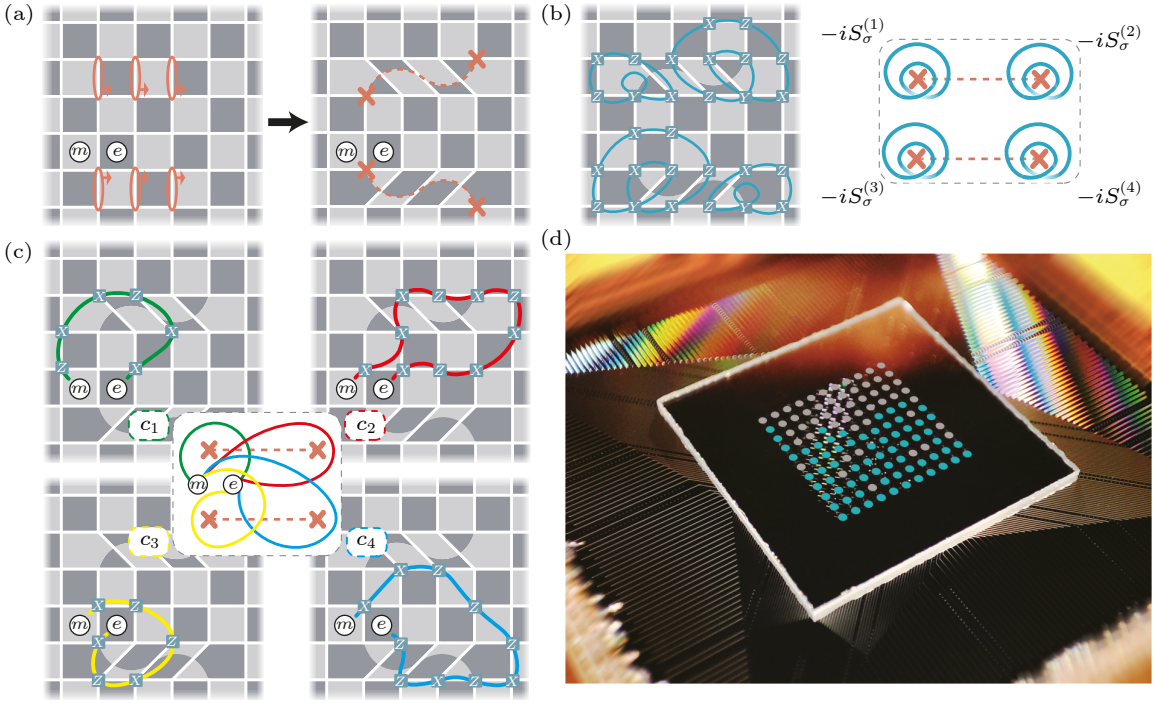

Fig. 1. Simulating non-Abelian anyons with twists and the photograph of the experimental quantum processor Ⅰ. (a) The deformation of the toric-code model with two pairs of twists, which behave as Ising anyons under braiding and fusion. Two Abelian topological charges e and m are illustrated, with e anyons living on the dark plaquettes and m anyons on the light ones. The twists are formed by rearranging the circled bonds and marked with the cross symbol $\times$. (b) The string operators $-iS_\sigma$ that specify the generalized charge of the non-Abelian twists. The fusion rules between the twists and other charges can be demonstrated by using these operators. In the right panel, we use a conceptual figure to sketch the relative positions of the twists and the corresponding string operators, omitting the details of the lattice sites and the constitutive local Pauli operators for simplicity and better illustration. (c) Four Majorana operators used to describe the four non-Abelian twists and the corresponding conceptual figure. The fusion and braiding of non-Abelian twists can be conveniently implemented with these operators. [18] (d) A photograph of the superconducting quantum processor Ⅰ with the chosen 68 qubits used in our experiment highlighted in cyan.

Framework and Experimental Setups. We consider the toric-code model with qubits living on the vertexes of a square lattice described by the following Hamiltonian: [11,43]

$$H = -\sum_{\boldsymbol{k}} \boldsymbol{A}_{\boldsymbol{k}}, \quad \boldsymbol{A}_{\boldsymbol{k}} = X_{\boldsymbol{k}} Z_{\boldsymbol{k}+\boldsymbol{i}} Z_{\boldsymbol{k}+\boldsymbol{j}} X_{\boldsymbol{k}+\boldsymbol{i}+\boldsymbol{j}}. \tag{1}$$

Here $\boldsymbol{k} = (a, b)$ indexes the spins in the a-th row and b-th column, and $\boldsymbol{i} = (1, 0)$, $\boldsymbol{j} = (0, 1)$. X, Y, and Z are Pauli operators. Noting that all the plaquette operators $\boldsymbol{A}_{\boldsymbol{k}}$ commute with each other, the ground state of this Hamiltonian can be simply described by the condition $\langle \boldsymbol{A}_{\boldsymbol{k}} \rangle = 1$ for all $\boldsymbol{k}$. There are two types of quasiparticle excitations (corresponding to $\langle \boldsymbol{A}_{\boldsymbol{k}} \rangle = -1$), dubbed e anyons (or "electric charges") living at the dark plaquettes and m anyons (or "magnetic charges") living at the light plaquettes, respectively [see Fig. 1(a)]. These are Abelian anyons, [11,43] and they can be created and moved by string operators, which are products of sequences of Pauli operators, as shown in Fig. 1(b). When an e anyon is fused

with an m anyon, one obtains an ϵ particle that behaves as a fermion. For our purpose of simulating non-Abelian anyons in a digital fashion, we consider introducing dislocations in the lattice.[18,44] For instance, in Fig. 1(a) we deform the lattice so as to obtain two pairs of pentagonal plaquettes, and modify the Hamiltonian with new pentagonal plaquette operators accordingly. After the deformation, each pentagonal plaquette hosts a twist, which involves a lattice site that is shared by three (rather than four) neighboring plaquettes. As shown in Fig. 1(c), due to the dislocation a string winding around a twist cannot close, and consequently an e anyon winds around a twist will become an m anyon or vice versa. Theoretically, it has been predicted that twists resemble non-Abelian Ising anyons when braided and fused.[18]

Our experiments are performed on two flip-chip superconducting quantum processors I and Ⅱ. Processor I (Ⅱ) encapsulates 11×11 (6×6) frequency-tunable transmon qubits arranged in a square lattice, with tunable couplers connecting adjacent qubits. Each qubit capacitively couples to its own readout resonator for qubit state measurements. We select 68 (30) qubits on processor I (Ⅱ) to simulate non-Abelian anyons and their associated braiding statistics. Through optimizing device fabrication and controlling process, we push the median lifetime of the qubits on processor I (Ⅱ) to 109.8 μs (139.8 μs) and the median simultaneous single- and two-qubit gate fidelities greater than 99.91% and 99.4% (99.95% and 99.5%), respectively. The chosen 30 qubits on processor Ⅱ form a regular rectangular lattice and the desired twists are artificially created to some extent. Yet, the 68 qubits on processor I are more irregularly distributed due to limited capacities in both wirings of our dilution refrigerator and measurement electronics, and twists can be constructed by taking advantages of the imperfect geometry. In the main text, we mainly discuss the results obtained from processor I [Fig. 1(d)], so as to stress that our approach for simulating non-Abelian anyons bears the merit of generally applicable to quantum processors with unintended imperfections. The experiments carried out on processor Ⅱ yield similar results we present in the Supplementary Materials for completeness and comparison.

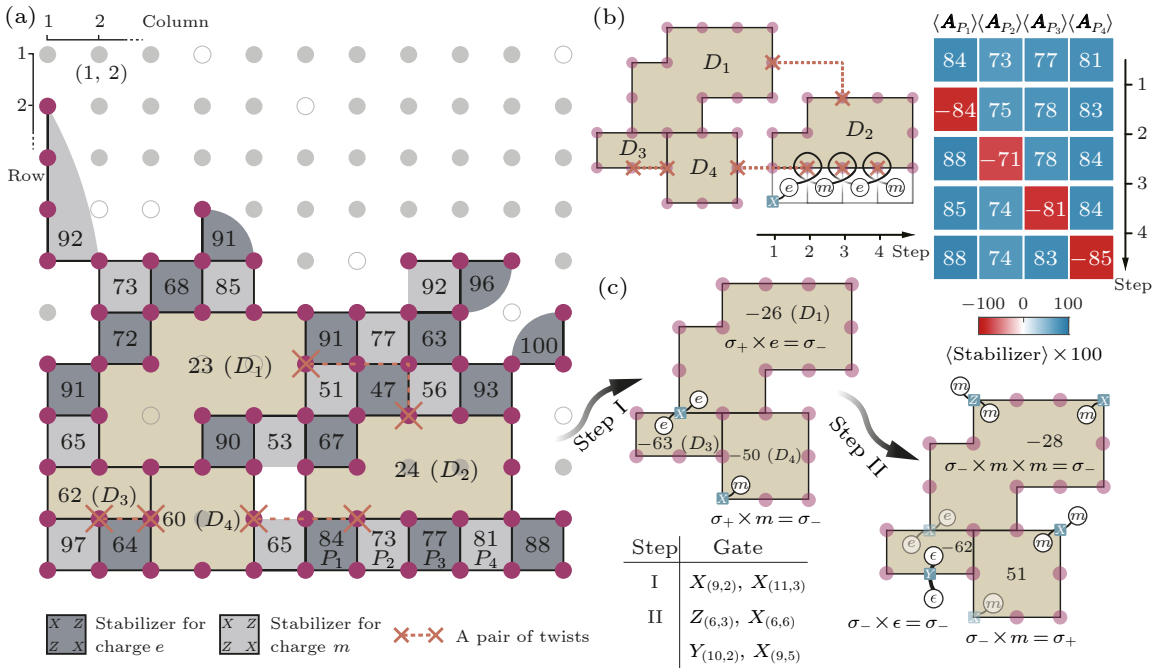

Fig. 2. The processor I and demonstration of the fusion rules. (a) Layout of the processor and the measured stabilizer values of the deformed toric-code ground state. The purple dots represent the chosen qubits used in our experiment, whereas the grey (white) dots denote the functional but unused (non-functional) qubits. The black line connecting two adjacent qubits shows where a controlled-Z (CZ) gate can be implemented. The dark (light) grey plaquettes host e (m) anyons, and the brown blocks denote the natural defects explored in our experiment to implement twists. The stabilizer for the smallest square reads $\boldsymbol{A_k} = X_k Z_{k+i} Z_{k+j} X_{k+i+j}$, and that for each defect is the product of all $\boldsymbol{A_k}$ it encloses. The three pairs of crosses connected by dashed lines denote the six twists used to simulate non-Abelian anyons. The integer number in each plaquette shows the corresponding measured stabilizer value (in percentage) of the prepared deformed toric-code state. (b) The sketch of the defects with eight twists. In the experiment, we create an e anyon by applying the gate $X_{(11,6)}$ and then move it to wind around the three marked twists below D_2 successively. We measure the four stabilizers ($\boldsymbol{A}_{P_1}$, $\boldsymbol{A}_{P_2}$, $\boldsymbol{A}_{P_3}$, and $\boldsymbol{A}_{P_4}$) at each step and their corresponding values are shown in the right panel. (c) Demonstration of the fundamental fusion rules. We initialize the system to be a ground state with the generalized charges being i for the chosen six twists marked in (a) ($S_\sigma = i$, corresponding to six σ_+ twists, see Ref. [18] and also see section I-D in the Supplementary Materials). We then create e, m, and ϵ quasiparticles, and measure the stabilizer values corresponding to the defects, which specify the fusion results. The integer numbers in the defects show the measured stabilizer values (in percentage), respectively. In the lower left panel, the table indicates the Pauli operations used to generate the quasiparticles.

Topological Charges and Fusion Rules. We first demonstrate the simulation of both Abelian and non-Abelian anyons and the fundamental fusion rules. Based on the geometric structure for the chosen 68 qubits on processor I and the available connections between them, we use a quantum circuit with a circuit depth of 43 (containing 294 single-qubit rotations and 113 two-qubit controlled-Z gates, see Fig. S12) to prepare the ground state of the corresponding stabilizer Hamiltonian (Supplementary Materials I-G). In Fig. 2(a), we sketch the geometric structure of the chosen 68 qubits and plot the individual stabilizer values measured after the ground state preparation. We achieve an average stabilizer value of 0.73, which is notable given the fact that certain stabilizers involve multi-qubit (up to 14 qubits) measurements. The deviation between the ideal theoretical prediction and experimental result is mainly attributed to limited gate fidelity and coherence time. All stabilizer values are positive, implying that there are no anyon excitations for the ground states. Also see Fig. S14 for experimental results from processor Ⅱ, where an average stabilizer value of 0.86 is obtained.

With twists, the system can host six generalized topological charges:[18] $\mathbf{1}$, e, m, ϵ, σ_+, and σ_-. They obey the following fundamental fusion rules:

$$\begin{aligned} &\sigma_\pm \times e = \sigma_\pm \times m = \sigma_\mp,\ \sigma_\pm \times \epsilon = \sigma_\pm, \\ &\sigma_\pm \times \sigma_\pm = 1 + \epsilon,\ \sigma_\pm \times \sigma_\mp = e + m, \end{aligned} \tag{2}$$

which can be verified using proper string operators. In our experiments, we demonstrate only some of the fusion rules for simplicity and concreteness. The remaining fusion rules either follow trivially or can be demonstrated in a similar way. After preparing the ground state of the Hamiltonian with twists, we create an e anyon and move it to wind around the twists located at the bottom of the D_2 defect [Fig. 2(b)], through applying corresponding string operators on the relevant qubits. We measure the four stabilizers (labeled by $\boldsymbol{A}_{P_1}$, $\boldsymbol{A}_{P_2}$, $\boldsymbol{A}_{P_3}$, and $\boldsymbol{A}_{P_4}$) below D_2 at each step of this process and plot their values in the right panel of Fig. 2(b). It is clear that, at the beginning, all measured stabilizer values are positive, indicating that there is no anyon excitation in the system. After the creation of the e anyon, $\langle \boldsymbol{A}_{P_1} \rangle$ becomes negative, which indicates that there is an excitation at plaquette P_1 (an e anyon). This e anyon is then moved around the first twist and becomes an m anyon, which is confirmed in the experiment by the observation that $\langle \boldsymbol{A}_{P_2} \rangle$ becomes negative whereas $\langle \boldsymbol{A}_{P_1} \rangle$ changes back to be positive at step 2. The m anyon is further moved around the second twist and becomes an e anyon, as confirmed by the measured stabilizer values at step 3. At step 4, we further move the e anyon around the third twist and it becomes an m anyon again. This clearly shows that winding around an odd number of twists exchanges electric and magnetic charges. Also see Fig. S15 for experimental results from processor Ⅱ, where the fact that an e anyon winding around two twists will remain the same type is demonstrated as well.

In Fig. 2(c), we plot the measured results for $\boldsymbol{A}_{D_1}$, $\boldsymbol{A}_{D_3}$, and $\boldsymbol{A}_{D_4}$ (in the experiment, we have practically measured all the stabilizers. Here, for better illustration we only plot three of them that are most relevant for the discussion), which determine the topological charges for the relevant twists marked as crosses in Fig. 2(a) and hence verify the fusion rules. At the beginning, we prepare the system to the ground state of the stabilizer Hamiltonian, where all three measured stabilizer values are positive as shown in Fig. 2(a). In other words, the system possesses six σ_+ twists at the beginning. We then create a pair of e anyons and an m anyon by applying the X gate on both qubits at sites $(9, 2)$ and $(11, 3)$, respectively, as depicted in the left upper panel of Fig. 2(c). We measure the stabilizers $\boldsymbol{A}_{D_1}$, $\boldsymbol{A}_{D_3}$, and $\boldsymbol{A}_{D_4}$, and find $\langle \boldsymbol{A}_{D_1} \rangle = -0.265 \pm 0.015$, $\langle \boldsymbol{A}_{D_3} \rangle = -0.629 \pm 0.013$, and $\langle \boldsymbol{A}_{D_4} \rangle = -0.496 \pm 0.027$, consistent with two σ_- twists at the same positions where the original σ_+ twists live. This verifies the fusion rules $\sigma_+ \times e = \sigma_+ \times m = \sigma_-$.

We further create five m anyons and one pair of ϵ anyons, with their locations depicted in the right lower panel of Fig. 2(c). We find that $\langle \boldsymbol{A}_{D_1} \rangle$ and $\langle \boldsymbol{A}_{D_3} \rangle$ remain negative ($\langle \boldsymbol{A}_{D_1} \rangle = -0.281 \pm 0.012$ and $\langle \boldsymbol{A}_{D_3} \rangle = -0.620 \pm 0.005$), whereas $\langle \boldsymbol{A}_{D_4} \rangle = 0.510 \pm 0.017$ becomes positive. This demonstrates the fusion rules of $\sigma_- \times m = \sigma_+$ and $\sigma_- \times \epsilon = \sigma_-$. The demonstrated rule $\sigma_- \times \epsilon = \sigma_-$ implies that adding an ϵ quasiparticle to σ_- will not change the total topological charge, which reflects the fact that twists can act as sources and sinks for ϵ anyons. To study the braiding and fusion of two σ_+ twists, we define Majorana operators as string operators winding around twists with the same end points, as illustrated in Fig. 1(c) (see Supplementary Materials I-E). We measure the corresponding string operators and find that $\langle -ic_1c_2 \rangle$ can both be negative and positive as shown in Fig. 3, which verifies the nontrivial fusion rule $\sigma_+ \times \sigma_+ = \mathbf{1} + \epsilon$ for σ_+ twists. Also see Fig. S16 for the results from processor Ⅱ, where more fusion rules are demonstrated in a similar fashion.

We mention that, for the experiment carried out on processor I, several boundary qubits are involved in only one or two plaquettes so as to reduce the depth of the quantum circuits for preparing the ground state. This will increase the degeneracy of the ground states for the stabilizer Hamiltonian, but would not affect our purpose of demonstrating the fusion rules. The reason is that, in our experiment, we use a specific quantum circuit to prepare one of the ground states and a unitary protocol with measurements of only stabilizers involved in the Hamiltonian for the demonstration. As a result, other degenerate ground states are irrelevant and the missing boundary stabilizers will not affect the fusion results. This is confirmed by the agreement between the experimental results and theoretical predictions, and further verified by Fig. S16, where the same fusion results are obtained with a more regular geometry of the chosen 30 qubits and all boundary stabilizers added.

Braidings and Logic Gates. Braiding of non-Abelian anyons results in unitary operations in a space spanned by topologically degenerate states. This is the characteristic feature of non-Abelian anyons. As discussed above, we consider six σ_+ twists marked in Fig. 2(a). For simplicity

and convenience, we omit the symbol + and label them by σ_i $(i = 1, \ldots, 6)$, as depicted in Figs. 3(a) and 3(b). In general, braidings of twists can be implemented by adiabatically transforming the "geometry" of the Hamiltonian, Majorana tracking,[45] or code deformation.[46–48] Here, we implement braidings of the twists by Majorana tracking and code deformation (see Supplementary Materials I-F and I-H).

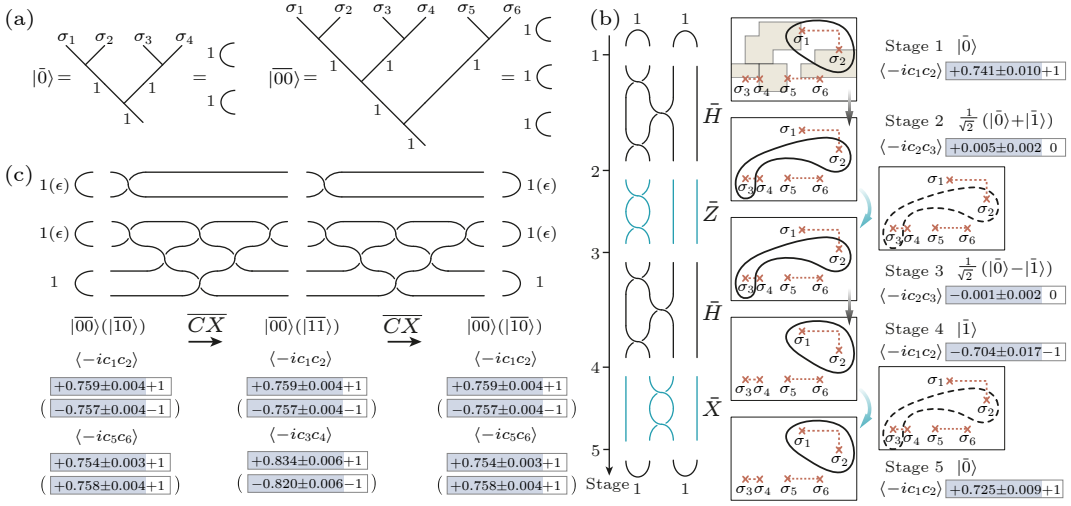

Fig. 3. Encoding of logical qubits with twists and demonstration of logic gates. (a) The encoding scheme described with fusion trees.[6] Here, for succinctness we only show part of the encoded logical bases $|\bar{0}\rangle$ and $|\overline{00}\rangle$ (Supplementary Materials I-F). (b) On the left shows the braiding sequence corresponding to the process of $\bar{X}\bar{H}\bar{Z}\bar{H}|\bar{0}\rangle = |\bar{0}\rangle$, with $\bar{H}$ realized by Majorana tracking (black lines) and other operations realized by implementing the corresponding string operators on physical qubits (blue lines). Time flows from up to down. The top middle panel sketches the defects and the three pairs of twists (denoted by σ_i, $i = 1, 2, 3, 4, 5, 6$), with the black solid circle denoting the string operator of the logical $\bar{Z}$ observable (corresponding to the Majorana correlator $-ic_1c_2$) for the first logical qubit. During the braiding procedure, the correspondence between the logical $\bar{Z}$ observable and Majorana correlator may change according to Majorana tracking, as outlined in the lower four panels in the middle column. The right column shows the logical states at each stage, which are verified by measuring the Majorana correlators corresponding to logical $\bar{Z}$ observable, with the experimental (shaded values with error bars) and ideal (unshaded integers) results following. The data are presented as mean values ± standard error of the mean with a sample size of five. The two black dashed circles sketch the string operators applied to the physical qubits, which correspond to the logic $\bar{Z}$ and $\bar{X}$ gates, respectively. (c) The braiding sequence corresponding to applying two logic controlled-X ($\overline{CX}$) gates consecutively on the state $|\overline{00}\rangle$ or $|\overline{10}\rangle$. Time flows from left to right. We measure the corresponding Majorana correlators at each step and show their measured values in the lower panel. See Supplementary Materials I-F for details.

In Fig. 3, we illustrate how frequently used single- and two-qubit gates can be carried out on the encoded logical qubits. Given that the total topological charge is **1**, the six σ twists can be used to encode two logical qubits. In Fig. 3(a), we illustrate the encoding scheme used in our experiment. We first show how single-qubit gates can be implemented for the first logical qubit, through braiding the first three twists. To this end, in Fig. 3(b) we show the braiding sequence to implement the unitary circuit $\bar{X}\bar{H}\bar{Z}\bar{H}|\bar{0}\rangle$ and our experimental results on measuring the relevant Majorana correlations after the application of each gate. We prepare the system in the logical $|\bar{0}\rangle$ state. We measure the Majorana correlation $\langle -ic_1c_2\rangle$, which corresponds to measuring the fusion charge of σ_1 and σ_2. We find $\langle -ic_1c_2\rangle = 0.741 \pm 0.010$, which is consistent with the fact that the system is in the logical $|\bar{0}\rangle$ state initially. A Hadamard gate on the first logical qubit can be applied by sequential braidings of σ_1 and σ_2, σ_2 and σ_3, and then σ_1 and σ_2 again. This process is in turn equivalent to changing fusion basis, which corresponds to F- and R-moves in the language of topological quantum computing,[6] and can be verified through measuring $-ic_2c_3$. In our experiment, we obtain $\langle -ic_2c_3\rangle = 0.005 \pm 0.002$, which agrees well with the theoretical prediction of $\langle -ic_2c_3\rangle = 0$. The logic $\bar{Z}$ gate and $\bar{X}$ gate can be implemented by applying the string operators $-ic_2c_3$ and $-ic_1c_2$ on the physical qubits, respectively (Supplementary Materials I-F). Also see Figs. S17 and S18 for experimental results from processor Ⅱ, where the corresponding Majorana operators are explicitly shown and the braidings of twists by code deformation are demonstrated as well. The two-qubit logic controlled-X gate ($\overline{CX}$) can be implemented by the braiding operations shown in Fig. 3(c), which in turn is equivalent to a change of the fusion basis under the encoding scheme shown in Fig. 3(a). In order to demonstrate the action of $\overline{CX}$ gate, we prepare the system in either logical $|\overline{00}\rangle$ or $|\overline{10}\rangle$ state, and then apply sequentially two $\overline{CX}$ gates. We measure the corresponding Majorana correlations at each step. Our experimental results are shown in Fig. 3(c), which agree with the corresponding theoretical values. For the state $|\overline{00}\rangle$, applying the $\overline{CX}$ gate keeps it unchanged and thus the measured Majorana correlations

all remain positive. In contrast, for the state $|\overline{10}\rangle$, applying the $\overline{CX}$ gate evolves it to $|\overline{11}\rangle$, resulting in a sign flip for the relevant Majorana correlations. The deviation of the measured results from the ideal theoretical predictions is due to experimental imperfections and the fact that the measurements of the Majorana correlations are multiqubit nonlocal measurements.

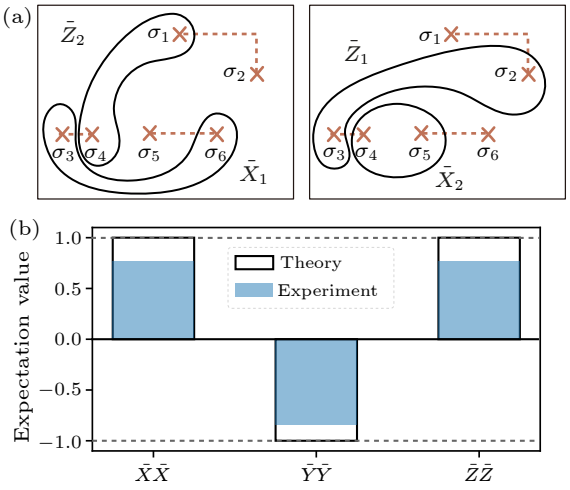

Fig. 4. Entangled logical state. (a) The sketch of the three pairs of twists and the string operators corresponding to the logical $\bar{Z}_1$, $\bar{Z}_2$, $\bar{X}_1$, and $\bar{X}_2$ operations (Supplementary Materials I-I). The encoding scheme is the same as that in Fig. 3(a). (b) Expectation values of $\bar{X}\bar{X}$, $\bar{Y}\bar{Y}$, and $\bar{Z}\bar{Z}$ for the entangled state of anyon-encoded logical qubits. The overlap between the experimentally prepared state $\rho_{\rm exp}$ with the ideal Bell state $|\overline{\Psi}\rangle = (|\overline{00}\rangle + |\overline{11}\rangle)/\sqrt{2}$, defined as $F = \langle\overline{\Psi}|\rho_{\rm exp}|\overline{\Psi}\rangle \equiv (1+\langle\bar{X}\bar{X}\rangle - \langle\bar{Y}\bar{Y}\rangle + \langle\bar{Z}\bar{Z}\rangle)/4$, is 0.844 ± 0.002.

Entangled Logical States. With the logic gates discussed above, we can prepare an entangled state for the logical qubits. To demonstrate this in experiments, we first prepare the system on the logical $|\overline{00}\rangle$ state in the same way as in Fig. 3(c). We then apply the logic Hadamard and $\overline{CX}$ gates to evolve the state to the logical Bell state $|\overline{\Psi}\rangle = (|\overline{00}\rangle + |\overline{11}\rangle)/\sqrt{2}$. In Fig. 4(a), we sketch the string operators corresponding to the logical $\bar{Z}_1$, $\bar{Z}_2$, $\bar{X}_1$, and $\bar{X}_2$ operations. We measure the expectation values of $\langle\bar{X}\bar{X}\rangle$, $\langle\bar{Y}\bar{Y}\rangle$, and $\langle\bar{Z}\bar{Z}\rangle$, and the results are shown in Fig. 4(b). From this figure, we obtain that the fidelity between the experimentally prepared logical state $\rho_{\rm exp}$ and the ideal Bell state $|\overline{\Psi}\rangle$ is 0.844 ± 0.002, which is larger than 0.5, indicating that the two logical qubits are entangled. We mention that, due to the particular encoding scheme used in our experiment, the procedure of preparing the Bell state in our experiment is in fact equivalent to a change of the fusion basis. Similarly, we exploit eight twists, four created by code deformation and the other four from the naturally existing ones at the corners, to encode three logical qubits and prepare a logical GHZ state on quantum processor Ⅱ (Fig. S19). In Fig. S19(A), we show the locations of the eight twists used and the corresponding string operators for logical $\bar{Z}_1$, $\bar{Z}_2$, $\bar{Z}_3$, $\bar{X}_1$, $\bar{X}_2$, and $\bar{X}_3$ observables. With these logical operators, we perform quantum state tomography for the prepared logical state and the result is displayed in Fig. S19(B), from which a fidelity of 0.771 ± 0.004 is obtained.

Discussion and Outlook. Although the braiding and fusion properties of twists resemble that of Ising anyons, they cannot be regarded as non-Abelian Ising anyons.[18] They are not intrinsic, finite-energy excitations of the system, and the unitary operation generated by braiding them is topologically protected only up to a nonuniversal overall phase. Thus, strictly speaking, the braiding statistics of the extrinsic twists is only well defined up to a phase, which is referred to as projective non-Abelian statistics in the literature.[16,49] We also clarify that all measurements in our experiment are destructive and the protocols are carried out without quantum error correction and thus are not endowed with topological protection in the strict sense. Achieving this requires consecutive non-destructive stabilizer measurements during the braidings of the twists, which is exceedingly challenging with a system size as large as 68 qubits for the state-of-the-art quantum technologies. The digital approach explored in our experiment is highly flexible and generally applicable to simulate a wide range of non-Abelian anyons. Recently, it has been shown theoretically that a broad family of non-Abelian states with a characterizing Lagrangian subgroup can be created efficiently through moderate-depth quantum circuits plus a single measurement layer.[25] This is within the reach of the current quantum technologies and it would be interesting to realize such non-Abelian topological orders and study their peculiar properties with programmable quantum processors as shown in this work. In addition, our digital simulation approach carries over readily to realizations of unconventional Floquet topological phases,[34,37] which also paves the way to simulating non-Abelian anyons and studying their unusual features in dynamically driven systems, such as these hosted by the Floquet color code[50] or Floquet spin liquids.[27]

Data Availability. The data presented in the figures and that support the other findings of this study are available for download at https://doi.org/10.5281/zenodo.7905826.

Acknowledgments. We thank L. M. Duan, X. Gao, S. T. Wang, and D. Yuan for helpful discussion. The device was fabricated at the Micro-Nano Fabrication Center of Zhejiang University. This work was supported by the National Natural Science Foundation of China (Grants Nos. 92065204, 12075128, T2225008, 12174342, 12274368, 12274367, U20A2076, and 11725419), the Innovation Program for Quantum Science and Technology (Grant No. 2021ZD0300200), and the Zhejiang Province Key Research and Development Program (Grant No. 2020C01019). Z.-Z.S., W.L., W.J., and D.-L.D. are supported by Tsinghua University, and the Shanghai Qi Zhi Institute.

References

[1] Griffiths D J and Schroeter D F 2018 *Introduction to Quantum Mechanics* (Cambridge: Cambridge University Press)

[2] MOTT N F 1968 *Rev. Mod. Phys.* **40** 677
[3] Tinkham M 2004 *Introduction to Superconductivity* (Courier Corporation)
[4] Dalfovo F, Giorgini S, Pitaevskii L P, and Stringari S 1999 *Rev. Mod. Phys.* **71** 463
[5] Wilczek F 1982 *Phys. Rev. Lett.* **49** 957
[6] Nayak C, Simon S H, Stern A, Freedman M, and Sarma S D 2008 *Rev. Mod. Phys.* **80** 1083
[7] Wilczek F 1990 *Fractional Statistics and Anyon Superconductivity* (Singerpore: World Scientific) vol 5
[8] Stern A 2010 *Nature* **464** 187
[9] Moore G and Read N 1991 *Nucl. Phys. B* **360** 362
[10] Wen X G 1991 *Phys. Rev. Lett.* **66** 802
[11] Kitaev A Y 2003 *Ann. Phys.* **303** 2
[12] Freedman M H, Larsen M, and Wang Z 2002 *Commun. Math. Phys.* **227** 605
[13] Sarma S D, Freedman M, and Nayak C 2006 *Phys. Today* **59** 32
[14] Stern A and Lindner N H 2013 *Science* **339** 1179
[15] Kitaev A 2006 *Ann. Phys.* **321** 2
[16] Barkeshli M, Jian C M, and Qi X L 2013 *Phys. Rev. B* **87** 045130
[17] Teo J C Y, Roy A, and Chen X 2014 *Phys. Rev. B* **90** 115118
[18] Bombin H 2010 *Phys. Rev. Lett.* **105** 030403
[19] Zheng H X, Dua A, and Jiang L 2015 *Phys. Rev. B* **92** 245139
[20] Brown B J, Laubscher K, Kesselring M S, and Wootton J R 2017 *Phys. Rev. X* **7** 021029
[21] Alicea J, Oreg Y, Refael G, von Oppen F, and Fisher M P 2011 *Nat. Phys.* **7** 412
[22] Ivanov D A 2001 *Phys. Rev. Lett.* **86** 268
[23] Bonderson P, Kitaev A, and Shtengel K 2006 *Phys. Rev. Lett.* **96** 016803
[24] Clarke D J, Alicea J, and Shtengel K 2013 *Nat. Commun.* **4** 1348
[25] Tantivasadakarn N, Verresen R, and Vishwanath A 2022 arXiv:2209.03964 [quant-ph]
[26] Liu Y J, Shtengel K, Smith A, and Pollmann F 2022 *PRX Quantum* **3** 040315
[27] Kalinowski M, Maskara N, and Lukin M D 2022 arXiv:2211.00017 [quant-ph]
[28] Deng D L, Wang S T, Sun K, and Duan L M 2015 *Phys. Rev. B* **91** 094513
[29] Banerjee M, Heiblum M, Umansky V, Feldman D E, Oreg Y, and Stern A 2018 *Nature* **559** 205
[30] Kasahara Y, Ohnishi T, Mizukami Y *et al.* 2018 *Nature* **559** 227
[31] Dolev M, Heiblum M, Umansky V, Stern A, and Mahalu D 2008 *Nature* **452** 829
[32] Bartolomei H, Kumar M, Bisognin R *et al.* 2020 *Science* **368** 173
[33] Satzinger K, Liu Y J, Smith A *et al.* 2021 *Science* **374** 1237
[34] Dumitrescu P T, Bohnet J G, Gaebler J P, Hankin A, Hayes D, Kumar A, Neyenhuis B, Vasseur R, and Potter A C 2022 *Nature* **607** 463
[35] Kyprianidis A, Machado F, Morong W *et al.* 2021 *Science* **372** 1192
[36] Mi X, Ippoliti M, Quintana C *et al.* 2022 *Nature* **601** 531
[37] Zhang X, Jiang W, Deng J *et al.* 2022 *Nature* **607** 468
[38] Acharya R, Aleiner I, Allen R *et al.* 2022 arXiv:2207.06431 [quant-ph]
[39] Zhao Y W, Ye Y S, Huang H L *et al.* 2022 *Phys. Rev. Lett.* **129** 030501
[40] Krinner S, Lacroix N, Remm A *et al.* 2022 *Nature* **605** 669
[41] Marques J F, Varbanov B M, Moreira M S *et al.* 2022 *Nat. Phys.* **18** 80
[42] Andersen T I, Lensky Y D, Kechedzhi K *et al.* 2022 arXiv:2210.10255 [quant-ph]
[43] Wen X G 2003 *Phys. Rev. Lett.* **90** 016803
[44] Kitaev A and Kong L 2012 *Commun. Math. Phys.* **313** 351
[45] Litinski D and von Oppen F 2017 *Phys. Rev. B* **96** 205413
[46] Dennis E, Kitaev A, Landahl A, and Preskill J 2002 *J. Math. Phys.* **43** 4452
[47] Raussendorf R, Harrington J, and Goyal K 2007 *New J. Phys.* **9** 199
[48] Bombin H and Martin-Delgado M A 2009 *J. Phys. A* **42** 095302
[49] You Y Z and Wen X G 2012 *Phys. Rev. B* **86** 161107
[50] Kesselring M S, de Fuente J C M L, Thomsen F, Eisert J, Bartlett S D, and Brown B J 2022 arXiv:2212.00042 [quant-ph]